

Compact 3D Map-Based Monocular Localization Using Semantic Edge Alignment

Kejie Qiu, Shenzhou Chen, Jiahui Zhang, Rui Huang, Le Cui, Siyu Zhu, and Ping Tan

Abstract—Accurate localization is fundamental to a variety of applications, such as navigation, robotics, autonomous driving, and Augmented Reality (AR). Different from incremental localization, global localization has no drift caused by error accumulation, which is desired in many application scenarios. In addition to GPS used in the open air, 3D maps are also widely used as alternative global localization references. In this paper, we propose a compact 3D map-based global localization system using a low-cost monocular camera and an IMU (Inertial Measurement Unit). The proposed compact map consists of two types of simplified elements with multiple semantic labels, which is well adaptive to various man-made environments like urban environments. Also, semantic edge features are used for the key image-map registration, which is robust against occlusion and long-term appearance changes in the environments. To further improve the localization performance, the key semantic edge alignment is formulated as an optimization problem based on initial poses predicted by an independent VIO (Visual-Inertial Odometry) module. The localization system is realized with modular design in real time. We evaluate the localization accuracy through real-world experimental results compared with ground truth, long-term localization performance is also demonstrated.

I. INTRODUCTION

With the fast development of large-scale 3D reconstruction and high-level autonomous driving, various 3D map productions have become widely available nowadays. Given a 3D map as the global localization reference, 6-DoF sensor pose (position and orientation) can be derived using specific pose estimation algorithms. Map-based localization is essentially a registration problem to match the sensor observations with a prior map. Usually high-quality sensors such as GPS-RTK (real-time kinematic), Lidar, and SINS (Strapdown Inertial Navigation System) are used for High Definition (HD) map construction, and low-cost sensors are used for localization. For example, a point cloud map constructed by a Lidar can not only be used for Lidar-based localization, but also a monocular camera-based localization approach [1]. A more general vision-based localization method is to utilize a map consists of a mass of visual features and their descriptors [2]. However, this map is difficult to maintain and the map size is too large for large-scale environments.

Besides point cloud maps and visual feature maps, there are many other map formats such as textured mesh model constructed by visual reconstruction, and even vector maps. Recently, the growing popularity of vector map standards such as OpenDrive¹ and NDS² indicates that a compressed

All the authors are with Alibaba A.I. Labs, Hangzhou, China. kejie.qkj@alibaba-inc.com.

¹<http://opendrive.org>

²<http://nds-association.org/>

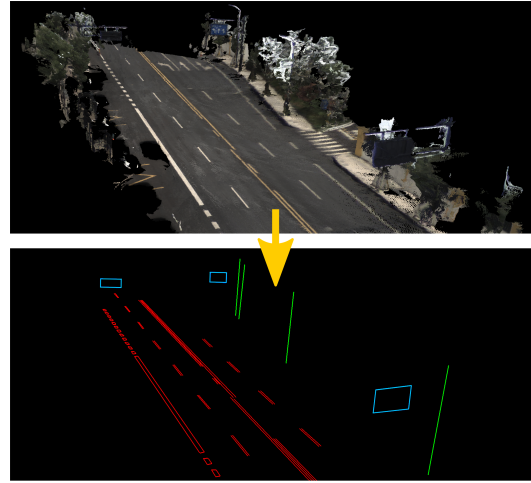


Fig. 1: Map compaction using the proposed compact map format in an urban environment. The map size is significantly reduced while the key landmarks are reserved using two types of line segments (a line segment & a wireframe). Each type can be labeled with multiple semantic categories.

map is a tendency for a light-weight and scalable map representation. To make full use of available 3D maps, we propose to use a more compact map that only consists of semantic line segments and wireframes. Because plenty of structural elements exist in man-made environments and many of them are comprised of straight line segments, such as lane lines, lamp poles, traffic signs in outdoor environments (Fig. 1), as well as windows, ceilings, and walls in indoor environments. Thanks to the compact representation, the proposed compact map can be generated from various HD maps of man-made environments. Also, the map size can be further reduced for on-board and large-scale deployment.

Visual localization, as a low-cost and light-weight solution, has attracted significant study these years, especially the monocular solutions. However, a monocular camera lacks direct range measurement, and the traditional point features are easily affected by perspective and illumination changes. To overcome this problem, edge features are used in a model-based localization system [3]. Because of the rapid development of learning-based perception, real-time object detection [4] and semantic segmentation [5], [6], [7] can help improve the robustness of visual feature-based localization. In fact, semantic features have been used in multiple incremental and global localization systems [8], [9]. Compared with the widely used semantic point cloud or semantic objects, the proposed semantic edges achieve to balance both compactness and accuracy.

In this paper, we propose a visual localization solution based on a compact map and a low-cost sensor set consists of a monocular camera and an IMU, which can be mounted on vehicles, robots, and hand-held devices to realize real-time global localization. With semantic perception, the extracted edge features are marked with specific semantic labels for robust feature association and accurate pose estimation.

We identify our contributions as follows:

- We propose a light-weight map format consisting of semantic line segments and wireframes, which can be generated from various 3D maps and take very little storage space.
- We adopt semantic edges to achieve robust feature association and potentially higher accuracy compared with other semantic elements.
- We implement the localization system in real-time to validate the localization performance using real-world experiments.

II. RELATED WORK

Map-based visual localization is a state estimation problem about how to register visual observations to a pre-constructed 3D map, a great number of works about this topic have been studied in the past few years. According to whether or not a prior camera pose is needed, the localization algorithms can be divided into *independent localization* and *prior-based localization*.

Independent localization is also known as relocalization or loop closure detection of simultaneous localization and mapping (SLAM). An inquiry image is the only input and the absolute camera pose is estimated. For example, it can be realized by establishing 2D-3D correspondences between the image pixels and the 3D points of the map, followed by a Perspective-n-Point (PnP) solver [10], [11], [2]. However, these methods require feature descriptors to be stored in the map, resulting in large map sizes. In practice, an image retrieval algorithm or a rough position range can also be utilized to speed up the feature match process. Recently, end-to-end regression networks are used to solve visual localization in small-size environments [12], [13], but they cannot generalize to new scenarios.

Prior-based localization, on the other hand, depends on an initial camera pose for accurate camera pose estimation. Landmarks are selected from the map according to the initial pose for feature alignment, it is then formulated as an optimization problem by iteratively minimizing the alignment cost [14], [15], [16]. Thus, in addition to an inquiry image, a prior camera pose is needed to make the optimization successfully converged. This method does not need image descriptors for image-level match because of the use of the prior camera pose, and has various feature alignment approaches in addition to descriptor-based alignment. For instance, Zuo *et.al* propose to align the semi-dense point cloud provided by a stereo camera with a prior Lidar map [17], and Caselitz *et.al* utilize the sparse points generated by monocular visual bundle adjustment instead of a stereo camera [18]. The map size can be significantly reduced

compared with the map used by independent localization. Recently, several researchers propose to use a semantic map [9] or a vector map [15] as the key localization reference, and the map size can be further reduced.

The map used for localization and the visual features used for data association are highly related. Most traditional independent localization methods opt to utilize point features such as SIFT [19] and ORB [20], so the corresponding maps are represented with 3D feature points and their descriptors [2]. The prior-based localization methods prefer to use other alignment approaches instead of descriptor-based feature alignment. For instance, only a point cloud map is needed by using ICP (Iterative Closest Point) alignment [17], [18]. Besides point features, line features or edge features are also widely used. They are regarded to be more robust against perspective and illumination changes. [3] uses a textured mesh model as the reference map, and edge features could be extracted from the rendered images. [14] organizes the map as a set of road markings consists of solid and dashed lines for urban environment localization, in which the line features are directly used for feature association. Recently, semantic features have played an important role in robust data association, they are proved to be more stable and robust features because of the specific semantic information attached to the features. For urban environments, semantic elements like lane lines, lamp poles, traffic signs are represented in a self-defined format [16] or standard vector map format [15] for outdoor localization, while [9] builds a semantic point cloud map to represent guide signs, parking lines, speed bumps in parking lots for indoor localization. However, most map formats mentioned above are dedicatedly designed for a certain environment.

The proposed method belongs to the prior-based localization, and semantic edge features are used for observation-map registration. We propose to use a line segments-based map to represent the semantic edge features. Only the semantic edges can be represented by line segments and wireframes are used for map construction and localization landmarks, and this concise representation way is applicable to all man-made environments.

III. SYSTEM OVERVIEW

The proposed modular localization system includes a semantic segmentation module, a VIO module, a landmark selection module, a feature extraction module, and a semantic edge alignment module. We will focus on the last three modules in this paper. For system completeness, the compact map generation process is also briefly introduced in Section IV-A. Take the urban environment localization, for example, the localization pipeline is shown in Fig. 2. The localization system is initialized by a global reference such as GPS or other visual relocalization methods. Given a captured image, the semantic segmentation module first labels the image pixels semantically, without loss of generality, we segment the image into two kinds of semantic areas (road and non-road). According to the segmentation results, the potential dynamic image areas are masked out before further

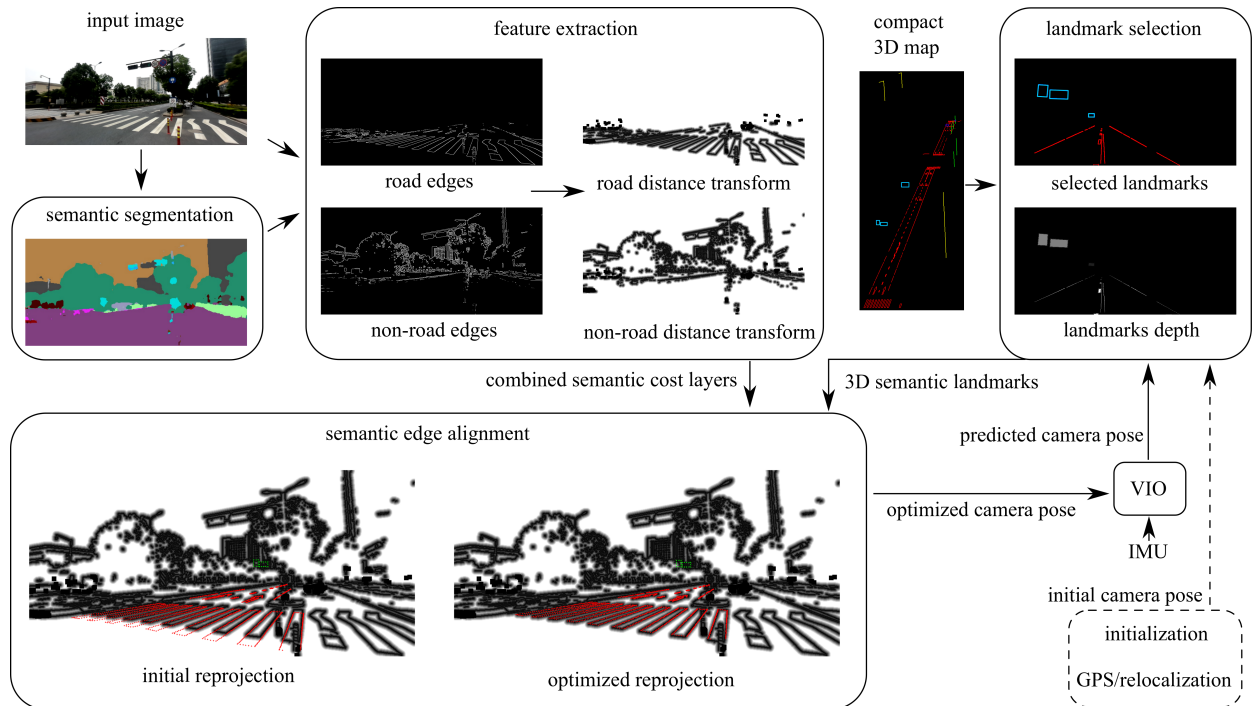


Fig. 2: The overall pipeline of the proposed map-based localization system. The whole localization system is initialized by a global reference shown in the dashed box, all the solid boxes denote modules running in real time. In the feature extraction module, semantic edge features are extracted from the input image considering the segmentation results, semantic energy maps (black: low energy; white: high energy) represented with distance transform are generated. In the landmark selection module, the landmarks for feature alignment are selected according to the prior camera pose provided by an independent VIO module. In the edge alignment module, the reprojections of the landmarks (color points) are illustrated before and after optimization.

processing, and the semantic edge features are extracted from the captured image using edge detection algorithms and the semantic segmentation results, the separate semantic edge images are turned into corresponding distance transforms for dense edge alignment. Meanwhile, the current camera pose is predicted according to the last camera pose and the odometry input from the VIO module. With the predicted camera pose, the corresponding landmarks are selected from the pre-constructed compact map for feature alignment. Finally, the global camera pose is derived within an optimization framework.

For the notations used in this paper, $(\cdot)^w$ is the world frame, $(\cdot)^r$ the prior camera frame for landmark selection, $(\cdot)^c$ the camera frame. \mathbf{t}_y^x and \mathbf{R}_y^x are the 3D translation and rotation of frame $(\cdot)^y$ with respect to frame $(\cdot)^x$. The skew-symmetric matrix operator is denoted as $[\cdot]_\times$. The focal lengths of the undistorted images are denoted as f_x and f_y , respectively. The corresponding image gradients of the distance transform are represented by G_u and G_v . $X(\mathbf{p})$, $Y(\mathbf{p})$, $Z(\mathbf{p})$ are the x , y , z values of a 3D point \mathbf{p} . Furthermore, we define the camera projection function $\pi: \mathbb{R}^3 \mapsto \mathbb{R}^2$ projects the 3D points onto 2D images.

IV. METHODOLOGY

A. Map definition & generation

We define two types of landmarks, namely, a line segment and a wireframe, each type can be attached with multiple semantic labels. A semantic line segment is represented by a

semantic label and two 3D points, and a semantic wireframe is represented by a semantic label and more than two 3D points (four points for a rectangle wireframe):

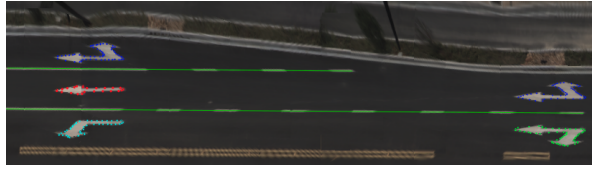
$$\text{Map} := \{\mathbf{L}_m | m=0,1,\dots, \mathbf{W}_n | n=0,1,\dots\}, \quad (1)$$

in which

$$\begin{aligned} \mathbf{L}_m &= \{s, \mathbf{p}_0, \mathbf{p}_1\}, \\ \mathbf{W}_n &= \{s, \mathbf{p}_0, \mathbf{p}_1, \mathbf{p}_2, \mathbf{p}_3\}, \end{aligned} \quad (2)$$

where s denotes a semantic label and $\mathbf{p} \in \mathbb{R}^3$ denotes a 3D point in the global coordinate. The used semantic labels depend on the specific application scenarios, for example, they will be road marks (lane lines, crosswalks, and other marks) on a road, lamp poles on roadsides, traffic signs above a road, and skylines generated by building edges in urban environments. Also, the map is compatible with indoor environments with different semantic labels.

As for map generation, the compact landmarks can be converted from standard map formats or generated from the results of multiple mapping algorithms using various sensors. For instance, based on an HD map constructed by visual dense mapping, the road marks can be efficiently detected in the inverse perspective mapping (IPM) images using a segmentation algorithm [21], as shown in Fig. 3(a). And the non-road elements can be firstly detected in the images using a dedicated neural network and secondly projected to the global coordinate with the help of corresponding depth information rendered from the mapping result, as shown in Fig. 3(b). In practice, both detection results can



(a) road mark detection



(b) non-road mark detection

Fig. 3: The road landmarks are detected in the IPM (bird's eye view) image while the non-road landmarks are detected in the normal image view.

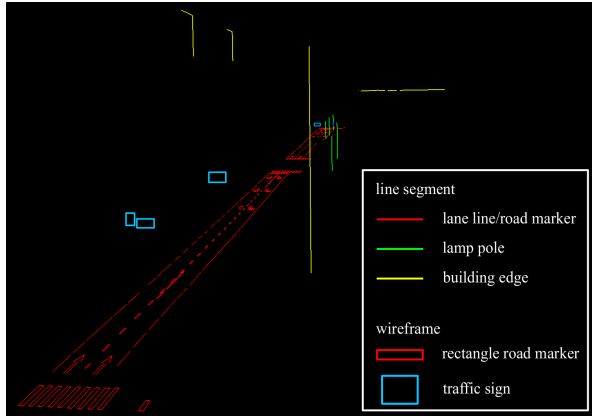


Fig. 4: Map generation of a sample urban environment.

be refined through manual annotation for better accuracy, and the landmarks shielded by vegetation are not kept. One sample compact map generation result is shown in Fig. 4.

B. Landmark selection

The landmarks used for prior-based localization are pre-selected from the map according to the prior camera pose $\mathbf{R}_r^w \mathbf{t}_r^w$. In fact, the predicted camera pose is computed by fusing the latest reliable localization results $\mathbf{t}_{c_l}^w$, $\mathbf{R}_{c_l}^w$, and the relative camera pose provided by the VIO module $\mathbf{t}_r^{c_l}$, $\mathbf{R}_r^{c_l}$:

$$\begin{aligned} \mathbf{t}_r^w &= \mathbf{t}_{c_l}^w + \mathbf{R}_{c_l}^w \mathbf{t}_r^{c_l}, \\ \mathbf{R}_r^w &= \mathbf{R}_{c_l}^w \mathbf{R}_r^{c_l}, \end{aligned} \quad (3)$$

where c_l is the latest frame with reliable localization result. In fact, only the landmarks within the prior camera field-of-view (FOV) are selected for feature alignment. Since the landmarks may be occluded by each other, we have to simulate the correct occlusion by considering the relative

position of the landmarks. For example, a traffic sign may cover the lamp poles or building edges behind it, and although the traffic sign is denoted by a wireframe consists of four separate line segments, the closed rectangle area is considered for depth buffering check. For the occlusion generated by the objects that appeared in the real sensing stage, we design a robust feature alignment method based on the semantic segmentation results, which will be detailed in the following content.

In fact, the landmark selection process is quite similar to the image rendering process in graphics: given a camera pose for image rendering, a virtual RGB image and its depth map are generated with correct occlusion simulation by using depth buffering, as shown in the landmark selection module of Fig. 2. Thus, we also make use of depth buffering to generate landmarks, because some of them may partially or completely be occluded by the landmarks in front of them. In particular, for a lamp pole, we first expand the line segment into a cylinder with an averaging pole radius for further landmark rendering. Finally, the visible landmark parts are sampled with sparse points on the corresponding edges in the rendered images for the following edge alignment.

C. Feature extraction & semantic edge alignment

The key feature alignment algorithm is based on matching semantic edge features with the corresponding semantic landmarks selected before. Given an image for localization, the edge features are detected by multiple edge detection algorithms, which are further segmented with the semantic segmentation results. The edges with the same semantic label are collected to formulate an edge image, then the corresponding semantic landmark points are reprojected onto the edge image, the residual term of the i th edge point of semantic label s (\mathbf{p}_{s_i} in the camera frame) is defined as the distance between the reprojected pixel and the nearest edge pixel:

$$r_{s_i}(\mathbf{R}_c^w, \mathbf{t}_c^w) = \min_j \mathbf{D}(\pi[\mathbf{R}_c^{wT}(\mathbf{R}_r^w \mathbf{p}_{s_i} + \mathbf{t}_r^w - \mathbf{t}_c^w)], \mathbf{u}_{s_j}), \quad (4)$$

where $\mathbf{D} : (\mathbb{R}^2, \mathbb{R}^2) \mapsto \mathbb{R}$ denotes the Euclidean distance between those points. If the 3D edge points are preselected then the minimization object function is exactly the definition of the distance transform [22]. It is generated from the corresponding edge image, as shown in the feature extraction module of Fig. 2. We denote the distance transform of the edge image as $V : \mathbb{R}^2 \mapsto \mathbb{R}$. The residual term of one specific edge point becomes

$$r_{s_i}(\mathbf{R}_c^w, \mathbf{t}_c^w) = V(\pi[\mathbf{R}_c^{wT}(\mathbf{R}_r^w \mathbf{p}_{s_i} + \mathbf{t}_r^w - \mathbf{t}_c^w)]). \quad (5)$$

The overall energy term is formulated by accumulating all the edge point residuals with all the semantic labels:

$$e(\mathbf{R}_c^w, \mathbf{t}_c^w) = \sum_s \sum_i (r_{s_i}(\mathbf{R}_c^w, \mathbf{t}_c^w))^2. \quad (6)$$

Finally, the optimal camera pose estimation \mathbf{R}_c^w and \mathbf{t}_c^w can be derived by minimizing the overall energy term. To be specific, we use the minimal representation, namely $\xi \in$

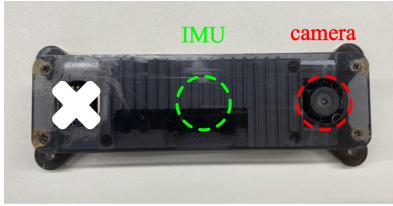


Fig. 5: The sensor set used for experiments. Only one camera and the inside IMU are used for the map-based monocular localization.

TABLE I: Timing statistics.

module	time	thread
semantic segmentation	49 ms	1
VIO	34 ms	2
landmark selection	8 ms	3
feature extraction & alignment	37 ms	4

se(3) instead of \mathbf{R}_c^w and \mathbf{t}_c^w for optimization implementation, and we apply the Gaussian Newton method to solve this optimization problem:

$$\mathbf{J}^T \mathbf{J} \delta \xi = -\mathbf{J}^T r(0), \quad (7)$$

where \mathbf{J} is the stacked matrix of all \mathbf{J}_{s_i} pixel-wise Jacobians with a specific semantic label.

The key Jacobian with regard to the error state $\delta \xi$ is computed as follows:

$$\mathbf{J}_{s_i} = \frac{\partial \mathbf{r}_{s_i}}{\partial \mathbf{p}_{s_i}} \frac{\partial \mathbf{p}_{s_i}}{\partial \delta \xi}, \quad (8)$$

where

$$\frac{\partial \mathbf{r}_{s_i}}{\partial \mathbf{p}_{s_i}} = \begin{bmatrix} G_u f_x / Z(\mathbf{p}_{s_i}) \\ G_v f_y / Z(\mathbf{p}_{s_i}) \\ -G_u f_x X(\mathbf{p}_{s_i}) / Z(\mathbf{p}_{s_i})^2 - G_v f_y Y(\mathbf{p}_{s_i}) / Z(\mathbf{p}_{s_i})^2 \end{bmatrix},$$

$$\frac{\partial \mathbf{p}_{s_i}}{\partial \delta \xi} = [-\mathbf{R}_c^{wT} \mid [\mathbf{R}_c^{wT} (\mathbf{R}_r^w \mathbf{p}_{s_i} + \mathbf{t}_r^w - \mathbf{t}_c^w)]_{\times}].$$

The camera pose ξ is updated by $\xi = \log(\exp(\xi)\exp(\delta\xi))$, then the camera pose \mathbf{R}_c^w and \mathbf{t}_c^w can be recovered from it if the optimization converges.

To further evaluate the localization results, we check the consistency of the estimated camera pose and the predicted camera pose, then drop the ones with large pose inconsistency. Also, we check the final averaging reprojection error, namely, the energy function value at the final iteration over the number of edge pixels, the estimations with large reprojection errors are also dropped. With the VIO module providing relative camera pose, the latest camera pose can be correctly predicted by skipping the dropped frames (Equation (3)). The proposed localization method is drift-free almost all the time, as long as the detected edge features and the selected landmarks are enough for pose estimation.

V. EXPERIMENTAL RESULTS

A. Implementation details

The compact maps used for experiments are generated from a dense point cloud map constructed by a high-end device including five industry cameras, one high-precision SINS and one wheel odometry mounted on a data acquisition

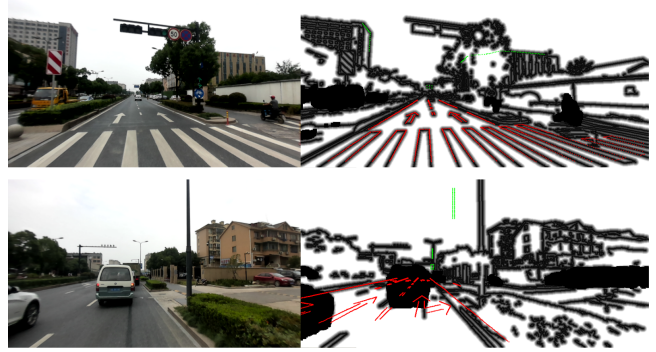


Fig. 6: Reprojections of selected 3D landmarks onto the captured images after optimization (the road and non-road distance transforms are combined, all the non-road landmarks are shown in green). First row: the reprojected landmarks match well with the detected edges, which means the optimization converges. Second row: the reprojected landmarks poorly match the detected edges, which means the optimization fails.

car. On the other hand, the sensor set used for localization includes the left monocular camera of an MYNT EYE camera which captures 640 by 400 images at 20 Hz and the internal IMU runs at 200Hz, as shown in Fig. 5. The intrinsic parameters of the camera and the extrinsic parameters between the camera and the IMU are calibrated in advance. The localization system is initialized with a visual relocalization method based on SuperPoint [10]. VINS-Mono [23] is used for monocular VIO implementation. DeepLabv3+ [5] with xception [24] model is used for semantic segmentation in urban environments, resulting road and non-road areas for further feature extraction. The whole localization system runs real-time on a desktop computer with an i7-8700K CPU and a GeForce GTX 1080 Ti graphics card, the detailed timing statistics are shown in Table I.

B. Localization evaluation

To vividly present the edge alignment results, we reproject the landmarks onto the composed distance transform that combines all the semantic layers for visualization, as shown in the semantic edge alignment module of Fig. 2. Normally, the reprojection landmarks (color points) are located in the low energy areas (black areas of the distance transform) after optimization. In other words, we can intuitively judge the localization results through the reprojection images.

TABLE II: Map statistics.

	trial 1	trial 2	trial 3	
landmarks number	419	144	74	
line segments	lane line	315	85	40
	lamp pole	5	3	5
	building edge	13	7	0
wireframes	rectangle mark	81	46	26
	traffic sign	5	3	3
road length	303 m	171 m	146 m	
original map size	220MB	184MB	69.4MB	
compact map size	25.2KB	9.2KB	4.9KB	
compression factor	8.9K	20.5K	14.5K	

The edge-based feature alignment is robust against illumination or appearance changes, and the usage of separated semantic feature layers further improves the convergence and accuracy. But there still exist several failure cases when the selected landmarks from the map are too few, or when severe occlusion occurs. For example, two reprojection images after optimization are shown in Fig. 6. If the landmarks are partially occluded, the rest landmarks still lead to correct pose estimation. However, if the landmarks are mostly occluded by other vehicles, the localization may fail to converge because the camera pose is not fully observable.

To evaluate the localization accuracy of the proposed method, we collect the localization data together with the high-end device which are all rigidly mounted on a data acquisition vehicle (the extrinsic parameters are calibrated in advance). The corresponding localization results are used as the ground truth for accuracy evaluation. There is nothing particular about the roads we select for experiments, pedestrians, riders, and many other vehicles are involved in the data acquisition process. Due to the semantic segmentation module, all potential dynamic objects are masked out from the camera view, the edge features are also marked for robust feature association. In the meantime, the VIO module keeps providing accurate relative pose prediction. As a result, the map-based localization survives from several occlusion situations.

Three trials of experimental data with a total length of 620m are collected together with the ground truth. The statistics of the compact maps used for localization are shown in Table II, the map of trial 1 has a relatively larger landmark density. Importantly, the map sizes are significantly reduced (compression factor = original map size/compact map size) with the compact map representation, which is beneficial to onboard systems and large-scale deployment.

The coordinate of the localization results has been unified to the world coordinate of the ground truth since the compact map is generated from the dense mapping result of the high-end device. We use Z-Y-X Euler angles for rotation representation. By considering the pre-calibrated extrinsic parameters, the pose estimation errors compared with the ground truth are shown in Fig. 7. The detailed numerical results evaluated with RMSE are shown in Table III. Due to the use of semantic edges instead of semantic objects, the proposed method achieves the position accuracy within 0.29m and the rotation accuracy within 0.52° , which satisfy the lane-level accuracy requirement of autonomous driving. Moreover, as shown in Table IV, we compare the proposed algorithm with other map-based algorithms using their reported localization accuracy, which shows the proposed method achieves the

TABLE III: RMSE of pose estimations.

trial	x (m)	y (m)	z (m)	norm (m)	yaw ($^\circ$)	pitch ($^\circ$)	roll ($^\circ$)	angle ($^\circ$)
1	0.15	0.21	0.10	0.29	0.19	0.31	0.15	0.46
2	0.23	0.12	0.12	0.29	0.20	0.41	0.25	0.52
3	0.10	0.22	0.09	0.26	0.12	0.17	0.20	0.29

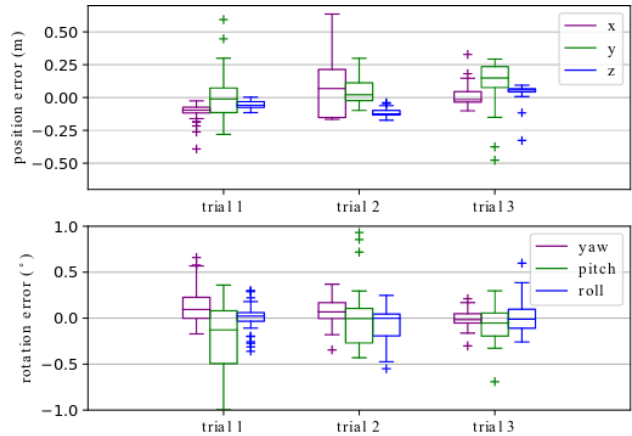


Fig. 7: Boxplot of the pose estimation error.

best performance level among the relevant works. More localization details are demonstrated in the attached video.

C. Long-term localization

In order to evaluate the long-term localization performance using the same compact map, we also collect the sensor data for localization four months later on the same road. The high-end device is not used this time, but the localization results can still be judged by checking the reprojection landmarks in the captured images with the estimated camera poses. For example, the day for mapping is a cloudy day and the road surface is dry, while the day for localization evaluation is a sunny day and the road surface is wet. Because of the robustness of the semantic edge features we use, the captured images can still be localized by only using the compact map constructed four months ago, more details are demonstrated in the attached video.

VI. CONCLUSION AND FUTURE WORK

In this paper, we propose a global localization system using monocular vision and inertial measurement based on a self-defined 3D compact map. The map consists of two types of landmarks: a line segment and a wireframe, each type with multiple semantic labels. An urban environment is used to illustrate methodology and evaluation. Moreover, thanks to the generalization of the defined map format, it can easily adapt to indoor environments or any man-made environments using specific semantic labels. In addition, the semantic edge features used for feature alignment are robust against perspective and illumination changes, resulting in long-term localization under the condition of complicated appearance changes. In the future, we will generate the

TABLE IV: Comparison of other methods.

methods	sensors	maps	position accuracy	rotation accuracy
[18]	camera	point cloud	0.30m	-
[25]	stereo camera	point cloud	0.60m	-
[16]	camera	line+point	0.35m	1.09°
[15]	camera	vector map	0.29m	-
ours	camera-IMU	line segment	0.29m	0.52°

compact map from other map formats and implement the localization system in other man-made environments.

REFERENCES

- [1] R. W. Wolcott and R. M. Eustice, "Visual localization within lidar maps for automated urban driving," in *2014 IEEE/RSJ International Conference on Intelligent Robots and Systems*. IEEE, 2014, pp. 176–183.
- [2] M. Bürki, I. Gilitschenski, E. Stumm, R. Siegwart, and J. Nieto, "Appearance-based landmark selection for efficient long-term visual localization," in *2016 IEEE/RSJ International Conference on Intelligent Robots and Systems (IROS)*. IEEE, 2016, pp. 4137–4143.
- [3] K. Qiu, T. Liu, and S. Shen, "Model-based global localization for aerial robots using edge alignment," *IEEE Robotics and Automation Letters*, vol. 2, no. 3, pp. 1256–1263, 2017.
- [4] J. Redmon and A. Farhadi, "Yolov3: An incremental improvement," *arXiv preprint arXiv:1804.02767*, 2018.
- [5] L.-C. Chen, Y. Zhu, G. Papandreou, F. Schroff, and H. Adam, "Encoder-decoder with atrous separable convolution for semantic image segmentation," in *Proceedings of the European conference on computer vision (ECCV)*, 2018, pp. 801–818.
- [6] H. Zhao, X. Qi, X. Shen, J. Shi, and J. Jia, "Icnnet for real-time semantic segmentation on high-resolution images," in *Proceedings of the European Conference on Computer Vision (ECCV)*, 2018, pp. 405–420.
- [7] C. Yu, C. Gao, J. Wang, G. Yu, C. Shen, and N. Sang, "Bisenet v2: Bilateral network with guided aggregation for real-time semantic segmentation," *arXiv preprint arXiv:2004.02147*, 2020.
- [8] S. L. Bowman, N. Atanasov, K. Daniilidis, and G. J. Pappas, "Probabilistic data association for semantic slam," in *2017 IEEE international conference on robotics and automation (ICRA)*. IEEE, 2017, pp. 1722–1729.
- [9] T. Qin, T. Chen, Y. Chen, and Q. Su, "Avp-slam: Semantic visual mapping and localization for autonomous vehicles in the parking lot," 2020.
- [10] D. DeTone, T. Malisiewicz, and A. Rabinovich, "Superpoint: Self-supervised interest point detection and description," in *Proceedings of the IEEE Conference on Computer Vision and Pattern Recognition Workshops*, 2018, pp. 224–236.
- [11] B. Zeisl, T. Sattler, and M. Pollefeys, "Camera pose voting for large-scale image-based localization," in *Proceedings of the IEEE International Conference on Computer Vision*, 2015, pp. 2704–2712.
- [12] E. Brachmann, A. Krull, S. Nowozin, J. Shotton, F. Michel, S. Gumhold, and C. Rother, "Dzac-differentiable ransac for camera localization," in *Proceedings of the IEEE Conference on Computer Vision and Pattern Recognition*, 2017, pp. 6684–6692.
- [13] E. Brachmann and C. Rother, "Learning less is more-6d camera localization via 3d surface regression," in *Proceedings of the IEEE Conference on Computer Vision and Pattern Recognition*, 2018, pp. 4654–4662.
- [14] Y. Lu, J. Huang, Y.-T. Chen, and B. Heisele, "Monocular localization in urban environments using road markings," in *2017 IEEE Intelligent Vehicles Symposium (IV)*. IEEE, 2017, pp. 468–474.
- [15] Z. Xiao, D. Yang, T. Wen, K. Jiang, and R. Yan, "Monocular localization with vector hd map (mlvhm): A low-cost method for commercial ivs," *Sensors*, vol. 20, no. 7, p. 1870, 2020.
- [16] Z. Xiao, K. Jiang, S. Xie, T. Wen, C. Yu, and D. Yang, "Monocular vehicle self-localization method based on compact semantic map," in *2018 21st International Conference on Intelligent Transportation Systems (ITSC)*. IEEE, 2018, pp. 3083–3090.
- [17] X. Zuo, P. Geneva, Y. Yang, W. Ye, Y. Liu, and G. Huang, "Visual-inertial localization with prior lidar map constraints," *IEEE Robotics and Automation Letters*, vol. 4, no. 4, pp. 3394–3401, 2019.
- [18] T. Caselitz, B. Steder, M. Ruhnke, and W. Burgard, "Monocular camera localization in 3d lidar maps," in *2016 IEEE/RSJ International Conference on Intelligent Robots and Systems (IROS)*. IEEE, 2016, pp. 1926–1931.
- [19] D. G. Lowe, "Distinctive image features from scale-invariant keypoints," *International journal of computer vision*, vol. 60, no. 2, pp. 91–110, 2004.
- [20] R. Mur-Artal and J. D. Tardós, "Orb-slam2: An open-source slam system for monocular, stereo, and rgb-d cameras," *IEEE Transactions on Robotics*, vol. 33, no. 5, pp. 1255–1262, 2017.
- [21] K. He, G. Gkioxari, P. Dollár, and R. Girshick, "Mask r-cnn," in *Proceedings of the IEEE international conference on computer vision*, 2017, pp. 2961–2969.
- [22] P. F. Felzenszwalb and D. P. Huttenlocher, "Distance transforms of sampled functions," *Theory of computing*, vol. 8, no. 1, pp. 415–428, 2012.
- [23] T. Qin, P. Li, and S. Shen, "Vins-mono: A robust and versatile monocular visual-inertial state estimator," *IEEE Transactions on Robotics*, no. 99, pp. 1–17, 2018.
- [24] F. Chollet, "Xception: Deep learning with depthwise separable convolutions," in *Proceedings of the IEEE conference on computer vision and pattern recognition*, 2017, pp. 1251–1258.
- [25] E. Stenborg, C. Toft, and L. Hammarstrand, "Long-term visual localization using semantically segmented images," in *2018 IEEE International Conference on Robotics and Automation (ICRA)*. IEEE, 2018, pp. 6484–6490.